

We are IntechOpen, the world's leading publisher of Open Access books Built by scientists, for scientists

5,800

Open access books available

142,000

International authors and editors

180M

Downloads

Our authors are among the

154

Countries delivered to

TOP 1%

most cited scientists

12.2%

Contributors from top 500 universities



WEB OF SCIENCE™

Selection of our books indexed in the Book Citation Index
in Web of Science™ Core Collection (BKCI)

Interested in publishing with us?
Contact book.department@intechopen.com

Numbers displayed above are based on latest data collected.

For more information visit www.intechopen.com



Chapter

An Experimental Investigation on the Thermodynamic Characteristics of DBD Plasma Actuations for Aircraft Icing Mitigation

Cem Kolbakir, Haiyang Hu, Yang Liu and Hui Hu

Abstract

We report the research progress made in our research efforts to utilize the thermal effects induced by DBD plasma actuation to suppress dynamic ice accretion over the surface of an airfoil/wing model for aircraft icing mitigation. While the fundamental mechanism of thermal energy generation in DBD plasma discharges were introduced briefly, the significant differences in the working mechanisms of the plasma-based surface heating approach from those of conventional resistive electric heating methods were highlighted for aircraft anti-/de-icing applications. By leveraging the unique Icing Research Tunnel available at Iowa State University (*i.e.*, ISU-IRT), a comprehensive experimental campaign was conducted to quantify the thermodynamic characteristics of a DBD plasma actuator exposed to frozen cold incoming airflow coupled with significant convective heat transfer. By embedding a DBD plasma actuator and a conventional electrical film heater on the surface of the same airfoil/wing model, a comprehensive experimental campaign was conducted to provide a side-by-side comparison between the DBD plasma-based approach and conventional resistive electrical heating method in preventing ice accretion over the airfoil surface. The experimental results clearly reveal that, with the same power consumption level, the DBD plasma actuator was found to have a noticeably better performance to suppress ice accretion over the airfoil surface, in comparison to the conventional electrical film heater. A duty-cycle modulation concept was adopted to further enhance the plasma-induced thermal effects for improved anti-/de-icing performance. The findings derived from the present study could be used to explore/optimize design paradigm for the development of novel plasma-based anti-/de-icing strategies tailored specifically for aircraft icing mitigation.

Keywords: DBD plasma actuation, Thermodynamics of DBD plasma discharges, Aircraft icing mitigation and protection

1. Introduction

Aircraft icing is widely recognized as one of the most serious weather hazards to flight safety [1–3]. Ice accumulation has been found to induce large-scale flow

separation over airframe surfaces, thereby, degrading the aerodynamic performance of an airplane significantly [4]. Ice accretion over airframe surfaces can make the aircraft to roll or pitch uncontrollably, and even causes crashes [5]. While considerable research progresses have been made in recent years to provide a better understanding about aircraft icing phenomena, preventing the loss of control due to ice accretion over airframe surfaces still remains an important unsolved problem at the top of National Transportation Safety Board (NTSB)'s most wanted list of aviation safety improvements as highlighted at <https://www.nts.gov/safety/mwl/Pages/mwl5-2017-18.aspx>.

It should be noted that, while anti-icing refers to the prevention of ice buildup on an airframe surface, de-icing denotes the scenario where ice has already formed on an airframe surface, which is removed subsequently. While a number of anti-/de-icing systems have been developed and implemented for aircraft icing mitigation in recent years, all aircraft anti-/de-icing systems can generally be classified into two categories: active and passive methods. While active methods rely on energy input from an external system for the anti-/de-icing operation, passive methods take advantage of the physical properties of the airframe surfaces (e.g., surface wettability) to prevent/delay ice formation and accretion. Current active anti-/de-icing strategies for aircraft icing mitigation suffer from various drawbacks. For example, spraying aqueous solutions of propylene and ethylene glycol (minimum of 50% concentration) along with other chemical additives are widely used for ground anti-/de-icing at airports before aircraft takeoff. Propylene and ethylene glycol, although readily biodegradable, exert an extremely high biochemical oxygen demand on aquatic systems that result in killing fish and other aquatic creatures due to the depletion of dissolved oxygen [6]. There has been an increasing concern of the environmental impacts from the aircraft de-icing fluid swept away with storm and melt water runoff at airports to ground water and nearby waterways [7]. Pneumatic de-icing systems with rubber boots have been used to break off ice chunks accreted at airfoil/wing leading edge for aircraft in-flight icing protection, but they are usually quite heavy and sometime unreliable [8]. Ultrasonic and mechanical de-icing solutions are not easily integrated into existing aircraft and pose foreign object damage (FOD) hazards to aero-engines [8]. While electric resistant heating or hot air bleeding systems have been used to melt out ice by heating airframe surfaces, they are usually very inefficient and have demanding power requirements and can also cause damage to composite materials from overheating. Furthermore, the melt water may simply run back and re-freeze at a downstream location to cause uncontrolled ice accretion [8]. Passive anti-icing approaches with hydro-/ice-phobic surface coatings have also been suggested as viable strategies for aircraft icing mitigation [9–11]. However, none of the passive approaches are found to be able to eliminate/prevent ice accretion over airframe surfaces completely, especially in the critical regions (e.g., near the airfoil leading edges) [12, 13]. Thus, it is highly desirable and important to develop novel and effective anti-/de-icing strategies to ensure safer and more efficient operation of aircraft under atmospheric icing conditions.

Dielectric barrier discharge (DBD) plasma actuators, which are fully electronic devices without any moving parts, have been studied extensively in the aerospace engineering community [14–16]. A DBD plasma actuator usually features two electrodes attached asymmetrically on the opposite side of a dielectric barrier layer. When a high voltage (i.e., either in alternating current (AC) or nanosecond pulses), is applied to the electrodes, the air over the encapsulated electrode will be ionized to generate a streak of plasma discharges. For AC-DBD plasma discharge, powered by an AC electric field, ionized air molecules is formed in the discharge region above the covered electrode inducing a fluid velocity adding momentum to

the boundary layer [17–20]. For the cases with the applied high voltages in nano-second pulses (i.e., ns-DBD plasma actuation), it would induce an ultrafast gas heating mechanism, leading to the generation of a shockwave [17–20]. The use of DBD plasma actuators has gained significant interest in the aerospace engineering community as a promising flow control tool to suppress airfoil stall [21–23] and eliminate separation of laminar boundary layer flows [24, 25] for improved aerodynamic performances. It should be noted that, even though DBD plasma actuators have been widely used for various flow control applications [26, 27], the electro-mechanical efficiency of DBD-plasma-based approach (e.g., the ratio of the energy used to induce ionic wall jet flows for flow control to the total energy consumed by the actuator) was found to be usually very low (i.e., no more than 0.20%) [28], and majority of the energy consumed by the plasma actuators would be dissipated via gas heating and dielectric heating [29].

As revealed clearly by Stanfield et al. [30] and Dong et al. [31], the rotational temperature of the gas above the grounded electrode of a DBD actuator during the plasma actuation can be increased up to 200°C, while the vibrational temperatures were observed to be an order of magnitude higher than the rotational temperature. It was also found that the primary mechanism for the heating of the dielectric layer is through heat transfer from the plasma, i.e., through direct injection, convection, and radiation. To further characterize the thermal effects of DBD plasma discharges, Tirumala et al. [32] used an infrared thermography technique to measure the surface temperature over a DBD plasma actuator, and found that the predominant mechanism of dielectric heating is due to the heat transfer from the plasma to the gas, which then heats up the dielectric surface through forced convection. The increase of the surface temperature was found to have linear relationship with both the applied voltage and the input frequency. By adopting the significant thermal effects of DBD plasma actuators, Cai et al. [33] conducted an explore study to demonstrate the feasibility of using plasma-induced thermal effects for anti-/de-icing operations by embedding an AC-DBD plasma actuator on an ice accreting cylinder model. The thermal effects of AC-DBD plasma actuation were found to be effective for both anti-icing and de-icing operations.

For the flow control applications on aircraft, DBD plasma actuators are usually designed to be mounted in the aerodynamically delicate regions where the aerodynamic characteristics would alter greatly as incoming flow changes (e.g., leading edges of wings and inlet lips of aeroengines) [14, 34]. It should be noted that, such aerodynamically delicate regions are usually also the preferential sites for ice formation and accretion [33]. Since DBD plasma actuation has been found to induce significant surface heating effects along with the ionic wind generation [30, 31], DBD plasma actuators can also be used promising candidates for aircraft icing mitigation. By leveraging icing research tunnels to generate icing conditions to simulate the dynamic ice accretion process over airfoil/wing surfaces, a series of experimental studies were conducted recently to demonstrate the feasibility of utilizing the plasma-induced thermal effects to suppress dynamic ice accretion process over the surfaces of airfoil/wing models for aircraft icing mitigation [29, 35–39].

In the present study, we report the research progress made in our research efforts to utilize the plasma-induced thermal effects to suppress dynamic ice accretion process over the surfaces of airfoil/wing models for aircraft icing mitigation. In the context that follows, while the fundamental mechanism of thermal energy generation in DBD plasma actuation is introduced briefly, the significant differences in the working mechanism of the plasma-based surface heating approach from those of conventional resistive electric heating methods for aircraft anti-/de-icing applications are highlighted. By leveraging the unique Icing Research Tunnel available at Iowa State University (i.e., ISU-IRT), a comprehensive experimental campaign is

conducted to quantify the thermodynamic characteristics of an DBD plasma actuator embed over the surface an airfoil/wing model exposed to frozen cold incoming air-flow with significant convective heat transfer in the context of aircraft anti-/de-icing. By embedding both a DBD plasma actuator and a conventional electrical film heater onto the surface of the same airfoil/wing model, an experimental investigation is also conducted to provide a side-by-side comparison between the DBD plasma actuator and the electrical film heater in preventing ice formation and accretion over the airfoil surface under a typical icing condition. While a high-speed camera is used to capture the transient details of the dynamic ice accretion and water transport processes over the airfoil surface, an infrared thermal imaging system is utilized to map the surface temperature evolutions during the dynamic ice accretion process or anti-/de-icing process with the AC-DBD plasma and the electrical film heater turned on. The temporally-synchronized-and-resolved IR thermal imaging results are correlated with the acquired ice accretion images to elucidate the underlying physics for a better understanding of the fundamentals of the DBD plasma-based approach for aircraft icing mitigation.

2. Mechanism of surface heating due to DBD plasma actuation

As that shown schematically in **Figure 1**, when a high voltage (i.e., either in alternating current (AC) or nanosecond pulses) is applied to the electrodes of an DBD plasma actuator, the air over the encapsulated electrode would be ionized to generate a streak of plasma charges. It has been reported that DBD plasma actuation would have significant thermal effects [24, 30–32, 40]. While substantial thermal energy is generated along with the formation of ionic airflow for AC-DBD plasma actuation [40], ns-DBD plasma discharge was found to induce an ultra-fast gas heating (FGH), which can dramatically affect the kinetics of chemical reactions, leading to the development of shockwaves in the near-surface gas layer [41–43].

It is well known that, when the high-voltages are applied to the electrodes, a high-intensity electric field would be generated between the exposed electrode and the grounded electrode separated by the dielectric layer. Driven by the electric field, the free electrons and ions in the air are responsible for energy transmission from the external power source to gas heating [32, 42]. As suggested by Popov [44] and Aleksandrov et al. [20], the dynamic gas heating during the plasma discharge is mainly caused by the complex collisions, reactions, and interactions between electrons, ions, and the excited molecules in the electrical field, as summarized in **Figure 2**.

The free electrons get energy from the electric field through acceleration, and then collide with neutrals and ions in the air. If an elastic collision occurs, there is an immediate, but only a rather small portion of total energy release, while in inelastic collisions, ionized particles and excited molecules can be produced, which are the main sources of energy heating the gas. Collision between ions and neutrals and

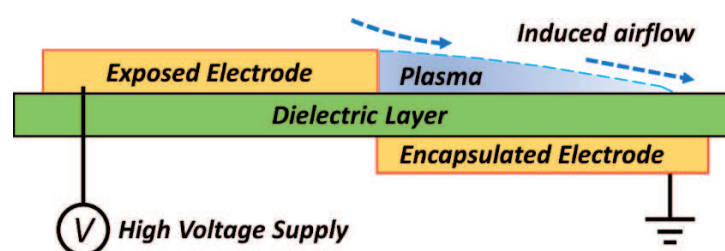


Figure 1.
Schematic of a typical DBD plasma actuator.

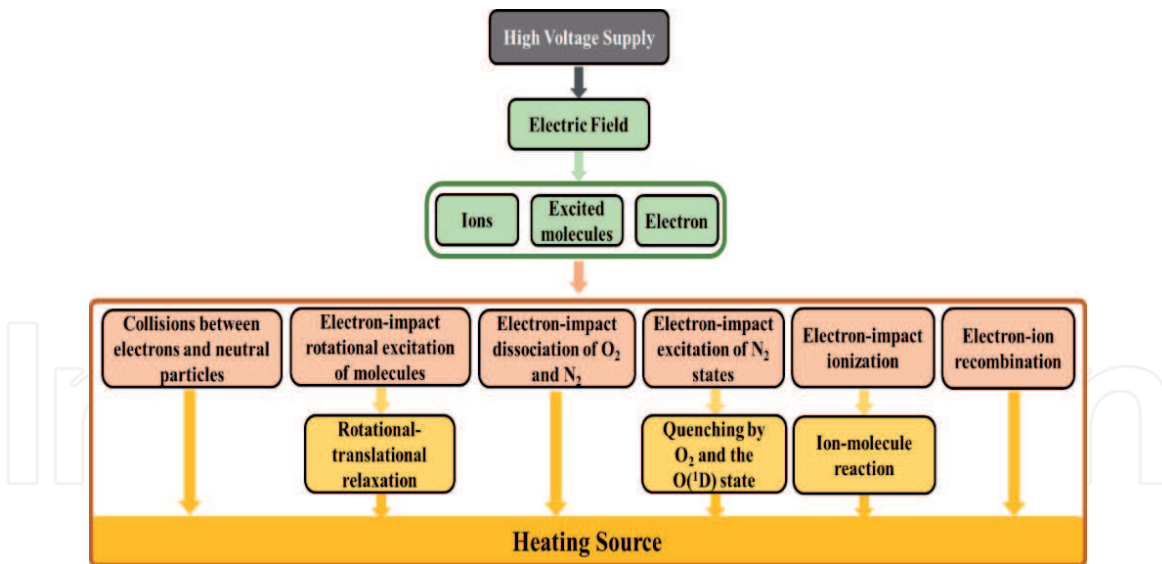


Figure 2.
 Heating mechanisms of DBD plasma actuation.

electrons is another source that should be taken into consideration [45]. **Figure 3** summarizes the primary reactions contributing to the gas heating in DBD plasma actuation. When the free electrons impact the molecules in the air (e.g., N_2 and O_2), these molecules would be excited from the ground states to the electronic states. Then, dissociation of the excited molecules would occur, which can generate a significant amount of thermal energy [44]. When electrons impact with the molecular ions in the electrical field, recombination would also occur [20], in which process, the energy would be released between the electronic and translational degrees of freedom of the produced atoms [44]. During the dissociation processes of the electronically excited molecules, while the energy released in the collisions is expended on the rotational excitation of molecules and gas heating, the rotational energy is relaxed into the translational degrees of freedom during the multiple collisions,

Molecule excitation from the ground state to the electronic states	$e + N_2 \rightarrow e + N_2^*$
	$e + O_2 \rightarrow e + O_2(B^3 \sum_u^-, v)$
	$e + O_2 \rightarrow e + O_2(A^3 \sum_u^+, C^3 \Delta_u)$
Dissociation of the excited molecules	$N_2^* \rightarrow N(^4S) + N(^2D) + \epsilon_R$
	$O_2(B^3 \sum_u^-, v) \rightarrow O(^3P) + O(^1D) + \epsilon_R$
	$O_2(A^3 \sum_u^+, C^3 \Delta_u) \rightarrow O(^3P) + O(^3P) + \epsilon_R$
Recombination when electrons impact with the molecular ions	$e + O_2^+ \rightarrow O(^3P) + O(^1D) + \epsilon_R$
	$e + NO^+ \rightarrow O(^3P) + N(^2D) + \epsilon_R$
	$e + N_2^+ \rightarrow N(^4S) + N(^2D) + \epsilon_R$
Quenching of the excited atoms	$O(^1D) + N_2 \rightarrow O(^3P) + N_2(v) + \epsilon_R$
	$O(^1D) + O_2 \rightarrow O(^3P) + O_2(b^1 \sum_g^+, v=2)$
Reaction of VT relaxation	$N_2(v) + O(^3P) \rightarrow N_2(v-1) + O(^3P) + \epsilon_R$

Figure 3.
 Primary reactions for gas heating in DBD plasma actuation.

which is termed as quenching of the excited molecules. The kinetic energy produced in the quenching processes is rapidly converted into gas heating [44]. It should be noted that, a large number of excited oxygen atoms are produced in the dissociation-recombination-quenching reactions. These excited atoms can also be quenched by the molecules in the air, i.e., N_2 and O_2 . It was suggested about 70% of the excitation energy of the excited atoms $O(^1D)$ is expended on gas heating [44]. Along with the above dissociation and quenching reactions, the excited oxygen atoms $O(^3P)$ would also lead to the reaction of VT relaxation, which is considered to be a significant reaction contributing to the gas heating [44].

3. Differences in the working mechanisms of the plasma-based approach from conventional resistive electric heating methods for aircraft inflight icing mitigation

Since the impingement of supercooled water droplets onto an airframe surface is the precursor for the ice accretion over the airframe surface, a better understanding about the heat transfer mechanisms during the impinging process of the water droplets onto the surface of a plasma actuator against that of a conventional electrical film heater is very helpful to elucidate the underlying physics to reveal the significant differences in the working mechanisms of DBD plasma-based approaches from those of conventional resistive electric heating methods for aircraft icing mitigation.

Figure 4 shows the schematics to reveal the great differences in the heating mechanisms as a water droplet impinging onto airfoil surfaces protected by using two different anti-/de-icing systems (*i.e.*, conventional electrical heating method *vs.* DBD plasma-based approach). For the case with a conventional electrical film heater, the thermal energy is generated on the heater surface through resistive electric heating as supplied from the electrical power source. While a portion of the thermal energy may be dissipated to the airflow above the heater surface due to the development of thermal boundary layer via convective heat transfer, which could warm up the impinging water droplet before it is in contact with the heater surface, the dominating mechanism for heating the water droplet would be through heat conduction after the dynamic impinging process (*i.e.*, droplet impacting, splashing, and receding), as

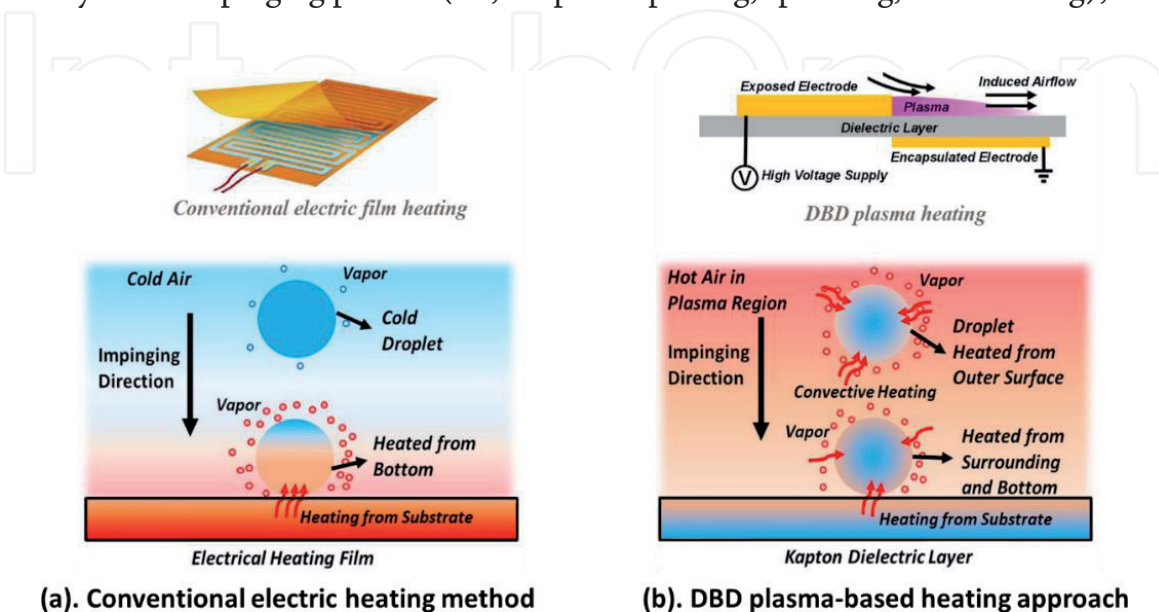


Figure 4. Comparison of different heating mechanisms as water droplet impinging onto the surface of an electrical film heater against that of a DBD plasma-based actuator.

shown schematically in **Figure 4(a)**. Due to the significant temperature differences between the impinging supercooled water droplet and the heater surface, the thermal energy would be transferred from the heater surface to the water droplet, which can keep the droplet warm up (*i.e.*, above the freezing point) or even being evaporated after the water droplet impacted onto the surface of the electric film heater.

However, as shown schematically in **Figure 4(b)**, the situation would become much different for the case as the water droplet impinging onto the airfoil surface protected by a DBD plasma actuator. As described in Tirumala et al. [32], the primary heating mechanism for plasma discharges is through heat transfer from the plasma to the ambient gas, which then heats up the dielectric surface through direct injection, convection and radiation. This is a reverse thermal path in comparison with that of the scenario of the conventional electrical heating method. Therefore, as the water droplet impinging onto the airfoil surface protected by the DBD plasma actuator, the water droplets would not only be heated up through heat conduction after impacted onto the hot dielectric surface, more importantly, but also be effectively heated up through forced convective heat transfer as the droplet traveling through the hot air in the plasma region even before becoming in contacting with the surface of the plasma actuator, as shown clearly in **Figure 4(b)**.

As described in Li *et al.* [46], the transient temperature of an in-flight droplet can be calculated by using equation of

$$T = \left[T_i - T_e + T_e \exp \left[\frac{(6t_f h)}{(\rho c_p D)} \right] \right] / \exp \left[\frac{(6t_f h)}{(\rho c_p D)} \right] \quad (1)$$

where T is the transient temperature of the in-flight droplet, h is the convection coefficient of air around the surface of the in-flight droplet, T_i is the initial temperature of the droplet, T_e is the air temperature surrounding the droplet, ρ is the density of the droplet, c_p is the specific heat of the droplet; t_f is the time of flight of the droplet in the convective air flow, and D is the diameter of the flying droplet. It is obvious that, with the same flight time, a higher temperature of the surrounding air would imply a higher transient temperature of the inflight water droplet. Since DBD plasma actuation would induce a significant gas heating above the surface of the plasma actuator, the temperature of the water droplet before impacting on the surface of the plasma actuator would become much higher than that of the case above the electrical film heater.

4. Evaluation of anti-/de-icing performance of the DBD plasma-based approach against conventional resistive electric heating methods for aircraft icing mitigation

As described above, even though both the DBD plasma-based approach and conventional electrical heating method utilize thermal energy to prevent the impinging supercooled water droplets from being frozen to cause ice accretion on the airframe surfaces, the fundamental working mechanisms of the two strategies are quite different for aircraft icing mitigation. It should also be noted that, the conventional electrical heating heaters usually have almost 100% energy efficiency in the sense that all the input electric energy would be converted to thermal energy, while the heating efficiency of DBD plasma actuation was found to vary from 50–90% under different operating conditions [47]. It is highly desirable to evaluate the overall effectiveness of the two different methods for aircraft anti-/de-icing applications. By embedding both a DBD plasma actuator and a conventional electrical film heater

onto the surface of the same airfoil/wing model, a comprehensive experimental campaign was conducted to provide a side-by-side comparison between the DBD plasma actuator and the conventional electrical film heater in preventing the ice formation and accretion over the airfoil surface.

4.1 Test model and experimental setup

The experimental study was performed in the Icing Research Tunnel available at Aerospace Engineering Department of Iowa State University (i.e., ISU-IRT). As shown schematically in **Figure 5**, ISU-IRT is a research-grade, multi-functional icing research tunnel with a test section of 2.0 m in length \times 0.4 m in width \times 0.4 m in height and four transparent side walls. It has the capacity of generating a maximum wind speed of 60 m/s in the test section and an airflow temperature down to -25°C . An array of eight pneumatic atomizer/spray nozzles are installed at the entrance of the contraction section of ISU-IRT to inject micro-sized water droplets ($10 \sim 100 \mu\text{m}$ in size) into the airflow. By manipulating the pressure and flow rate supplied to the atomizer/spray nozzles, the liquid water content (LWC) in ISU-IRT is adjustable (i.e., LWC ranging from 0.1 g/m^3 to 5.0 g/m^3). In summary, ISU-IRT can be used to simulate various atmospheric icing phenomena over a range of icing conditions (i.e., from dry *rime* to wet *glaze* ice conditions). In the present study, a typical glaze icing condition was generated in ISU-IRT with the freestream airflow velocity of $U_{\infty} = 40 \text{ m/s}$, temperature of $T_{\infty} = -5^{\circ}\text{C}$ and liquid water content level (LWC) of $\text{LWC} = 1.0 \text{ g/m}^3$.

Figure 5 also gives the schematic of the airfoil/wing model used in the present study, which has a NACA0012 airfoil profile in the cross section and a chord length of 150 mm (i.e., $C = 150 \text{ mm}$). A resistive electrical film heater (i.e., Kapton® Polyimide Film insulated heater), which was selected due to its outstanding operational performance among the electrical film heaters available on the market, was

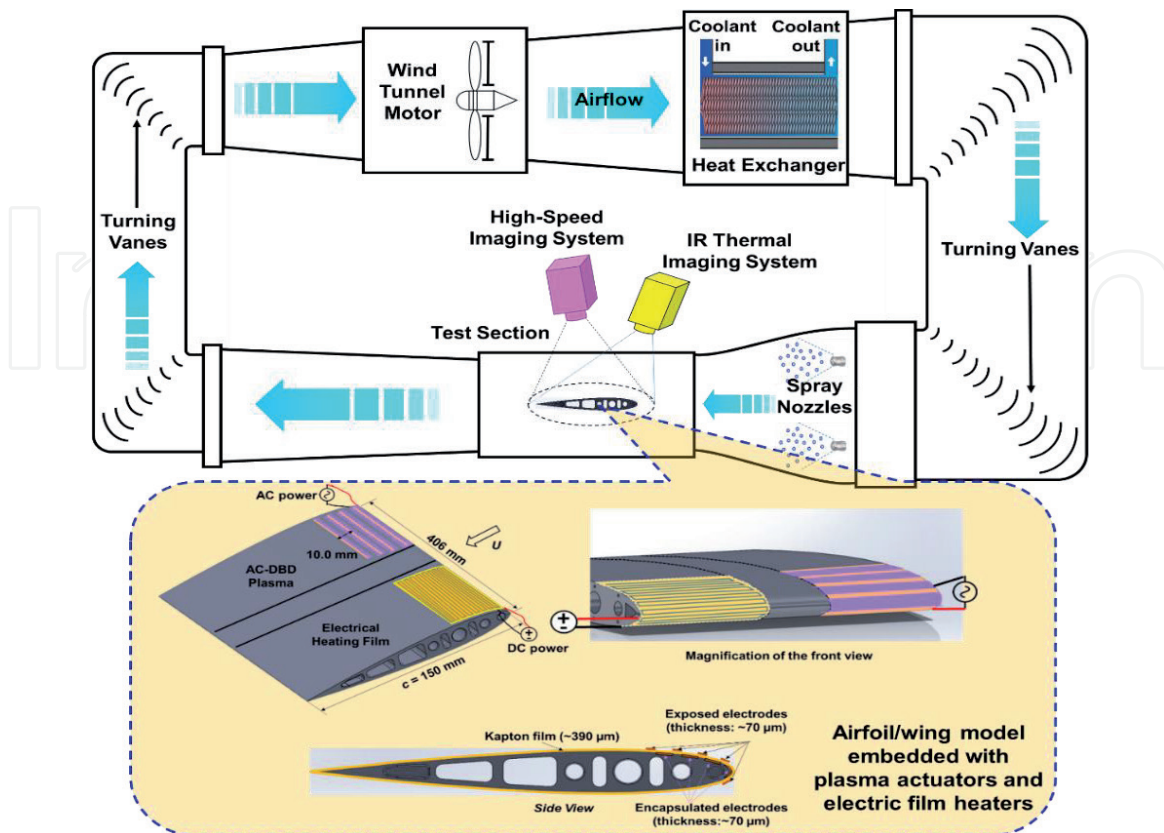


Figure 5. Schematic of ISU-IRT and the airfoil/wing model used for the experimental study.

embedded over one side of the airfoil surface. The electric film heater consists of an etched foil element of 0.013 mm thickness that is encapsulated between two layers of 0.05 mm Polyimide Film and 0.025 mm FEP adhesive tape. The coverage area of the film heater is 50.8 mm × 101.6 mm. A DC power source was used to power the electrical film heater for the anti-/de-icing operation during the experiments.

A DBD plasma actuator was embedded over the other half surface of the airfoil/wing model for a side-by-side comparison of the anti-/de-icing methods. The DBD plasma actuator consist of four encapsulated electrodes and five exposed electrodes, with the same electrode thickness of about 70 μm. Three layers of Kapton film (*i.e.*, 130 μm for each layer) were integrated to serve as the dielectric barrier to separate the encapsulated electrodes from the exposed electrodes. Ranging from the airfoil leading-edge to about 27% chord length downstream, four encapsulated electrodes were distributed evenly over the airfoil model with a separation distance of 3.0 mm. The length of the encapsulated electrodes was about 350 mm, and the width was 10.0 mm (except the one at the leading edge which was 5.0 mm). As reported by Waldman and Hu [48], since most of the ice would accrete around the leading edge of the airfoil/wing model, the width of the first encapsulated electrode was reduced to 5.0 mm in order to generate more plasma discharges near the airfoil leading-edge for a successful anti-/de-icing operation in the region, while the encapsulated electrodes were attached symmetrically around the leading edge of airfoil model. The exposed electrodes (*i.e.*, 96 mm in length and 3.0 mm in width) were placed right above the encapsulated electrodes with zero overlap between the exposed and encapsulated electrodes. The DBD plasma actuator were wired to a high-voltage AC power supply (Nanjing Suman Co., CTP-2000 K), which is capable of providing a maximum 30 kV peak-to-peak sinusoidal voltage with a center frequency of 10 kHz. During the experiments, while the AC current applied to the plasma actuator was measured by using a high response current probe (Pearson Electronics, Inc., Pearson 2877), the high-amplitude voltage was measured by using a high voltage probe (*i.e.*, P6015A from Tektronix). The electric voltage supplied to the electrodes was manipulated with a variable voltage transformer at a constant frequency of 10 kHz. In order to quantitatively compare the anti-/de-icing performance of the DBD plasma actuator against the electrical film heater under the pre-selected icing conditions, the applied power (*i.e.*, in the term of the applied power density, P_d) to the DBD plasma actuator was adjusted to be same as that applied to the electrical film heater.

During the experiments, in addition to use a high-speed, high-resolution camera (PCO Tech, Dimax) with a 60 mm lens (Nikon, 60 mm Nikkor f/2.8) to record the dynamic ice accreting or anti-/de-icing process over the airfoil surface, an infrared (IR) thermal imaging system (FLIR A615) was also used to map the surface temperature of the ice accreting airfoil surface via an infrared window (*i.e.*, FLIR IR Window-IRW-4C with optic material of Calcium Fluoride) flush mounted on the top wall of the ISU-IRT test section. An in-situ calibration was performed to validate the IR thermal imaging results against the measured surface temperature data with a high-accuracy RTD probe. The measurement uncertainty for the IR thermal imaging system was found to be within ±0.5°C. The high-speed video camera and the IR thermal imaging system were connected to a digital delay generator (Berkeley Nucleonics, model 575) that synchronized the timing between the two systems.

4.2 Thermodynamic characteristic of DBD plasma actuations under frozen cold conditions with significant heat convection pertinent to aircraft anti-/de-icing

As described above, while a number of investigations have been conducted to characterize the thermal effects of DBD plasma discharges [30–32, 40], almost all the previous studies were conducted in quiescent air at room temperature without

considering frozen cold conditions and significant convective heat transfer pertinent to aircraft icing phenomena. With the experimental set up described above, a comprehensive investigation was conducted to characterize the thermodynamic characteristics of DBD plasma actuators as a function of relevant controlling parameters (e.g., applied voltage, frequency, and power input, etc...) under frozen-cold test conditions coupled with significant convective heat transfer pertinent to aircraft anti-/de-icing.

Figure 6 shows one example of the experimental results to reveal the time evolution of the measured temperature distribution over the airfoil surface protected by the DBD plasma actuator a dry test condition (i.e., without turning on the water spray system of the ISU-IRT). For the experiment results, while the incoming airflow was set at of $U_\infty = 40$ m/s and $T_\infty = -5.0^\circ\text{C}$, the AC-DBD plasma actuators were supplied by AC voltage of $V_{p-p} = 12.5$ kV and $f = 10$ kHz, with the corresponding applied power density of $P_d = 7.8$ kW/m². It is clearly seen that, after the plasma actuator was switched on, the temperatures over the airfoil surface were found to increase rapidly, with the local surface temperatures at the edges of the exposed electrodes being raised from -5°C to more than 25°C in less than 5 seconds. As shown clearly in **Figure 6(a)**, the surface heating was first initiated at the edges of the exposed electrodes with evident local temperature peaks (i.e., as indicated by the white strips in the temperature map over the airfoil surface). As the time goes by, more and more thermal energy was generated during the plasma discharges, as seen from the measurement results shown in **Figure 6(b)–(d)**. It should be noted that the maximum temperatures were always found to be located at the edges of the exposed electrodes, which agrees with the findings reported in the previous studies [40]. Meanwhile, the temperature over the exposed electrodes (i.e., copper tap) appeared to be much higher than that over the dielectric layer (i.e., Kapton film). The temperature differences between the electrode surfaces and the surface of the dielectric layer were believed to be caused by the significant difference in the thermal conductivity between the copper tape and the Kapton film (i.e., 385.0 W/m·K for copper tape *vs.* 1.57 W/m·K for Kapton film). The measured surface temperature was found to be relatively low near the airfoil leading edge in general, and increased gradually at further downstream locations, which was correlated well with the chordwise development of the convective heat transfer over the airfoil surface (i.e., the heat convection would be maximum at the airfoil leading edge, and decrease gradually in the downstream [49]).

Based on the measured temperature distributions given in **Figure 6**, the spanwise-averaged temperature profiles along the airfoil chord can be extracted, and the extracted results are given in **Figure 7**. It can be seen clearly that the spanwise-averaged temperature profiles at the different time instances have a very similar distribution pattern, i.e., the surface temperatures were always found to reach the local peak values at the edges of the exposed electrodes, and then decrease gradually

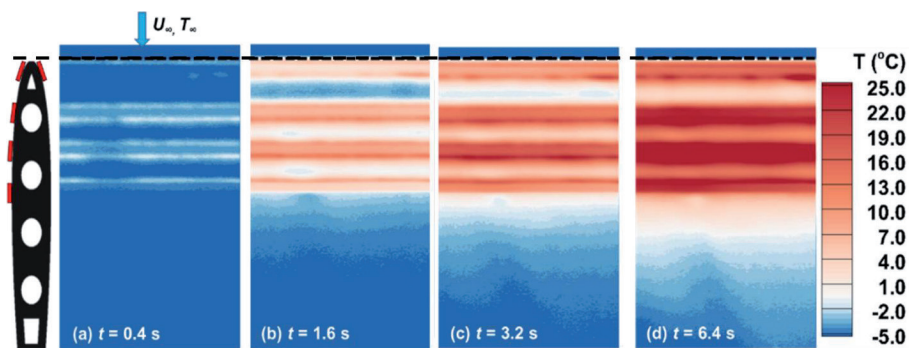


Figure 6. Measured temperature distribution over the airfoil surface with the DBD plasma actuator operating under a dry test condition of $U_\infty = 40$ m/s and $T_\infty = -5^\circ\text{C}$.

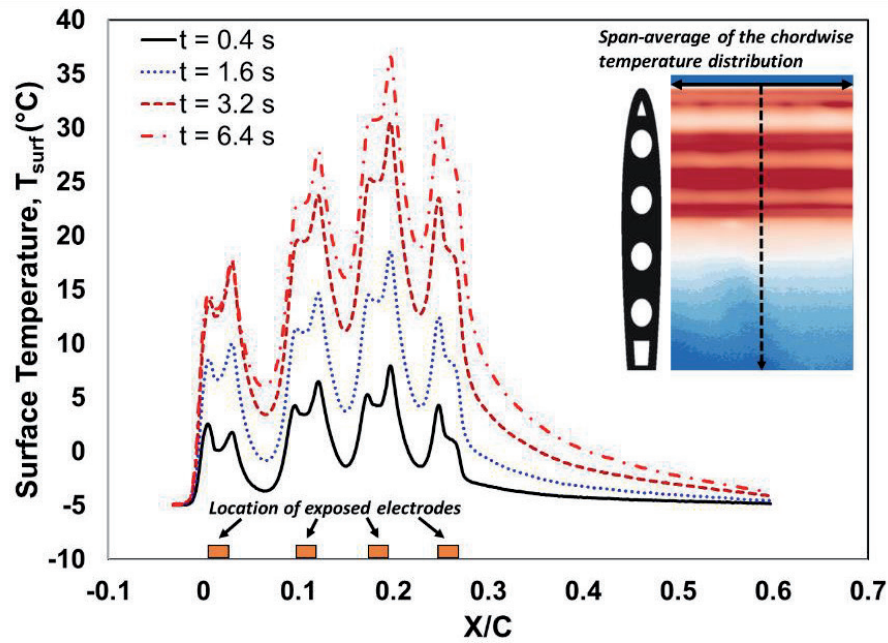


Figure 7. Spanwise-averaged temperature profiles along the airfoil chord with the DBD plasma actuators operating under a dry test condition of $U_{\infty} = 40$ m/s and $T_{\infty} = -5^{\circ}\text{C}$.

with the increasing distance away from the edges of the exposed electrodes. For example, at the time instance of $t = 0.4$ s, while the surface temperatures over the dielectric layer were found to have almost no change (i.e., still being frozen cold at $T_{\text{surface}} = -5^{\circ}\text{C}$), the local temperature peaks at the electrode edges were found to increase rapidly and become higher than $+5.0^{\circ}\text{C}$. Along with the rapid temperature rise at the edges of the exposed electrodes, the temperatures over the surfaces of copper-based electrodes were also found to become much higher in comparison to those over the dielectric layer. It was suggested that the predominant heating mechanism in plasma discharges is due to the heat transfer from the plasma to the gas, which then heats up the surface of the plasma actuator through forced convection [32]. With the plasma actuator embedded over the airfoil surface was exposed in the frozen cold airflow coupled with significant convective heat transfer, the hot air originally heated by plasma discharges would not only be in contact with the dielectric layer, but also convect over the copper-based exposed electrodes. It caused the temperature rise over the surfaces of the exposed electrodes. Due to the much higher thermal conductivity of the copper-based exposed electrodes, the electrode surfaces were found to have a much faster thermal response (i.e., rapid temperature increases) in comparison to that of the Kapton-based dielectric layer, as shown quantitatively from the measured temperature profiles given in **Figure 6**. As the time goes on, the temperatures over the airfoil surface were found to increase rapidly, with the maximum temperature raised to more than 35°C at 6.4 seconds after turning on the DBD plasma actuator. It can also be seen clearly that, the surface temperature around the third exposed electrode was found to be always higher than those at other locations, which is believed to be a result of the development of the thermal boundary layer over the airfoil surface, i.e., due to the effects of the significant convective heat transfer over the airfoil surface [50].

4.3 Comparison of the anti-/de-icing performance of the DBD plasma-based approach against the convention electrical surface heating methods

With the experimental setup given in **Figure 5**, a comprehensive experimental campaign was conducted to provide a side-by-side comparison of the DBD

plasma-based approach against conventional electrical heating methods in preventing the ice formation and accretion over the airfoil surface. In performing the ice accretion experiments, ISU-IRT was operated at a prescribed frozen-cold temperature level (e.g., $T_\infty = -5^\circ\text{C}$ for the present study) for at least 30 minutes in order to ensure ISU-IRT reaching a thermal steady state. Then, the DBD plasma actuator and the electrical film heater embedded over the airfoil/wing surface were switched on simultaneously for about 60 seconds to achieve a thermal equilibrium state before turning on the water spray system of ISU-IRT. After the water spray system was switched on at $t = t_0$, the super-cooled water droplets carried by the incoming airflow would impinge onto the surface of the airfoil/wing model to start the ice accretion process. During the experiments, the high-speed imaging system and IR thermal imaging system were synchronized to record the dynamic ice accretion or anti-/de-icing process and map the corresponding surface temperature distributions over the ice accreting airfoil/wing model simultaneously.

Figure 8 shows the typical snapshots of the dynamic ice accretion process over the airfoil surface with the same electric power supplied to the DBD plasma actuator and the electrical film heater (i.e., $P_d = 7.8 \text{ kW/m}^2$) for the anti-/de-icing operation. The box in red dashed lines in the acquired images indicates the measurement window of the IR thermal imaging system. Since very similar features were observed for all the test cases, only the measurement results obtained under the test conditions of $U_\infty = 40 \text{ m/s}$, $T_\infty = -5^\circ\text{C}$ and $LWC = 1.0 \text{ g/m}^3$ were shown and analyzed here for conciseness. As shown clearly in **Figure 8(a)**, right after starting the ice accretion experiments (i.e., $t = 10.0 \text{ s}$), since both the DBD plasma actuator and the electrical film heater had already been switched on for a while to make the surface temperatures of the airfoil/wing model being well above the freezing point of water, the supercooled water droplets were found to be heated up rapidly, upon impacting onto the heated airfoil surface. Therefore, the front surface of the airfoil model protected by the plasma actuator and the electrical film heater (i.e., from the leading edge to $\sim 30\%$ chord length) was found to be totally ice free, with evident water runback flow observed over the airfoil surface. Driven by the boundary layer airflow over the airfoil surface, the unfrozen water was found to run back in the form of film/rivulet flows. The runback water over the airfoil surface on the electrical film heater side was found to be refrozen into ice eventually to form rivulet-shaped ice structures at the downstream region of $X/C \approx 60\%$. In comparison,

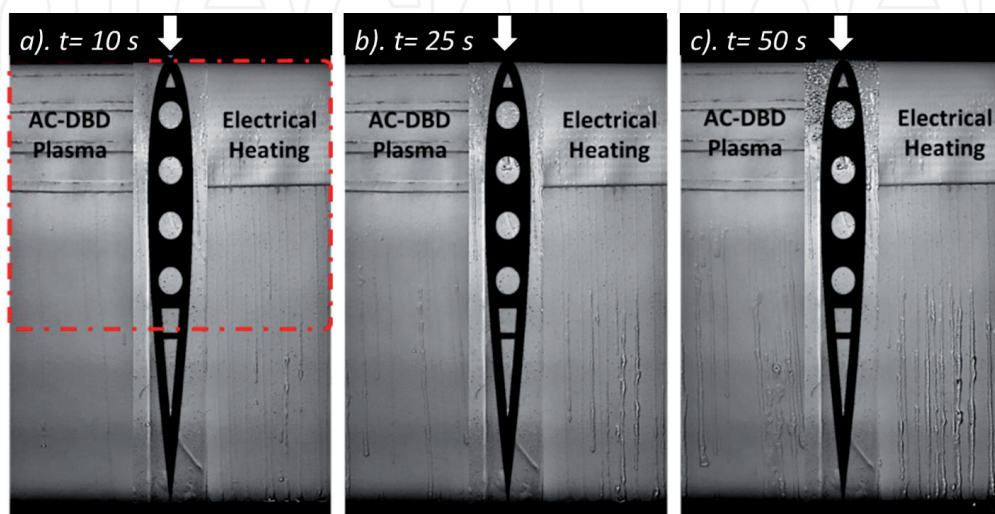


Figure 8. Acquired images to reveal the dynamic ice accretion process over the airfoil surface with the electric power supplied to the plasma actuator and the film heater being $P_d = 7.8 \text{ kW/m}^2$.

much less runback water was observed over the airfoil surface on the DBD plasma actuator side with much fewer ice structures formed at the downstream locations.

The experimental observation suggests that, with the same electric power inputs, the DBD plasma actuator seems to have a better anti-/de-icing performance in comparison to the conventional electric film heater. This can be explained by the facts that, since the airflow over the region covered by the DBD plasma actuator would be sufficiently heated due to the gas heating effects in the plasma activation, a portion of the airborne water droplets would be warming up rapidly and even evaporated as they flying through the plasma region before impacting onto airfoil surface, resulting in the less water mass collected over the airfoil surface protected by the DBD plasma actuator. However, with the supercooled water droplets impinging onto the airfoil surface protected by conventional electrical film heater, the thermal energy was mainly transferred from the heating elements to the airfoil surface via heat conduction. Since the input power for this cases was not sufficient to instantly evaporate the impacted water droplets (i.e., $P_d = 7.8 \text{ kW/m}^2$), the impacted water droplets were found to coalesce quickly on the airfoil surface to form rivulets/film flows to transport the impacted water mass to further downstream locations, as driven by the airflow over the airfoil surface. Due to the intense convective heat transfer between the surface water and the frozen cold incoming airflow over the airfoil surface, the runback water was found to be refrozen into ice eventually, result in the formation of rivulet-shaped ice structures at further downstream locations.

As the time goes on, more and more super-cooled water droplets would impinge onto the airfoil surface. As a result, more water mass was found to be collected over the airfoil surface to cause the formation of more rivulet-shaped runback ice accreted at the downstream locations of the airfoil surface. As shown in **Figure 8(b)** and **(c)**, while electric power supplied to the two systems were set to be the same value of $P_d = 7.8 \text{ kW/m}^2$, the ice structures accreted over the airfoil surface on the plasma actuator side were always found to be less than those on the electric film heater side.

In order to achieve a better anti-/de-icing performance, the electric power supplied to the plasma actuator and the electrical film heater were increased by a factor of two (i.e., $P_d = 15.6 \text{ kW/m}^2$) to generate more thermal energy for the anti-/de-icing. The typical snapshots of the dynamic water runback/ice accretion process with elevated power input are shown in **Figure 9**. It can be clearly seen that, with the higher power input of $P_d = 15.6 \text{ kW/m}^2$, the airfoil surface was found to become completely free of ice on both sides of the airfoil surface. It can also be seen that, similar to that observed for the case with relatively lower power input described above, the DBD plasma side of the airfoil surface appeared to have much less water runback in comparison to that on the electric film heater side. The rapid evaporation of the airborne water droplets as flying through the plasma region described above is believed to be the reason to cause the much less water mass collected on the plasma actuator side of the airfoil surface.

The corresponding IR thermal imaging results can reveal more details on the different working mechanisms of the two system for the anti-/de-icing operation. While **Figure 10** shows the time evolution of the measured temperature distributions over the airfoil surface before and after starting the ice accretion process, **Figure 11** gives the corresponding surface temperatures at different chordwise locations (i.e., locations of A, B, C and D at $X/C = 2.0\%$, 10% , 18% and 45% chord respectively, as indicated in **Figure 10**) as a function of the time on the two sides of the airfoil surface (i.e., plasma actuator side vs. electric film heater side). It can be seen clearly that, after the DBD plasma actuator was switched on for 10 seconds (i.e., at $t = 10\text{s}$), the temperatures over the exposed electrodes of the plasma

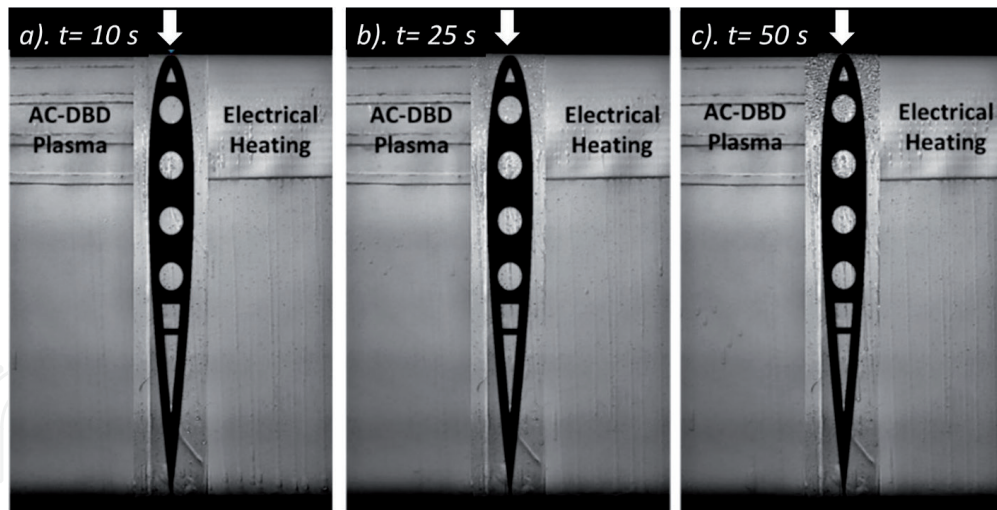
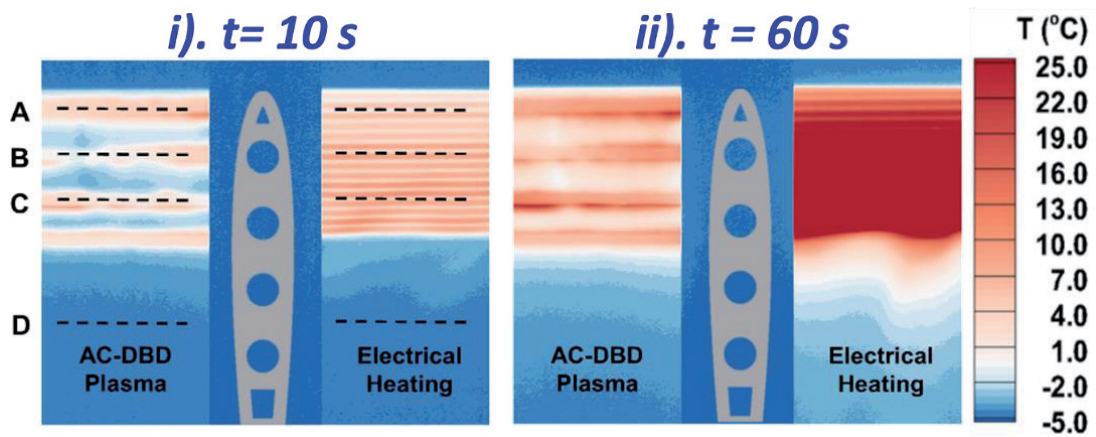
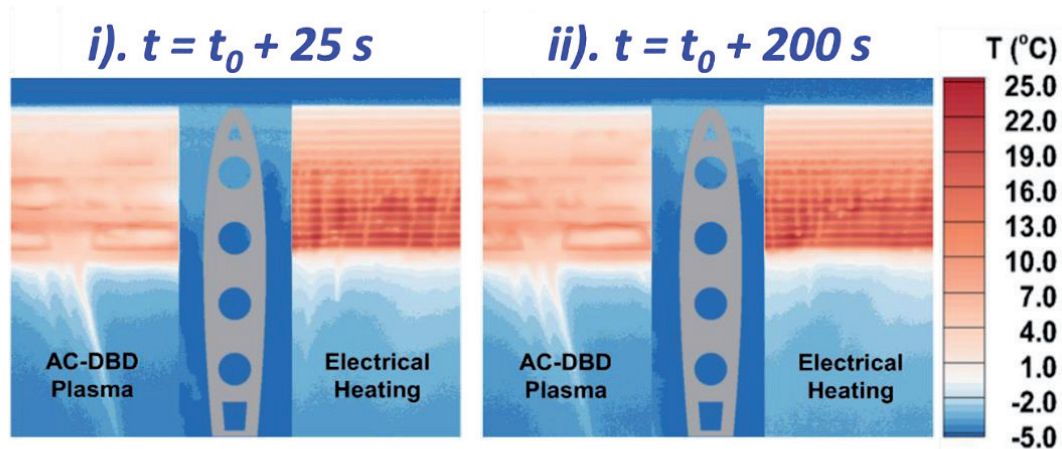


Figure 9. Acquired images to reveal the dynamic ice accretion process over the airfoil surface with the electric power supplied to the plasma actuator and the film heater being $P_d = 15.6 \text{ kW/m}^2$.



(a)



(b)

Figure 10. Time evolution of the measured temperature distributions over the airfoil surface before and after starting the ice accretion process.

actuator were found to increase to about 10°C , while the temperatures over the dielectric surface (*i.e.*, in the spacings between the electrodes) were still quite low (*i.e.*, below the freezing point of water), which has been discussed in the previous section. Since the electrical film heater was also switched on simultaneously, a

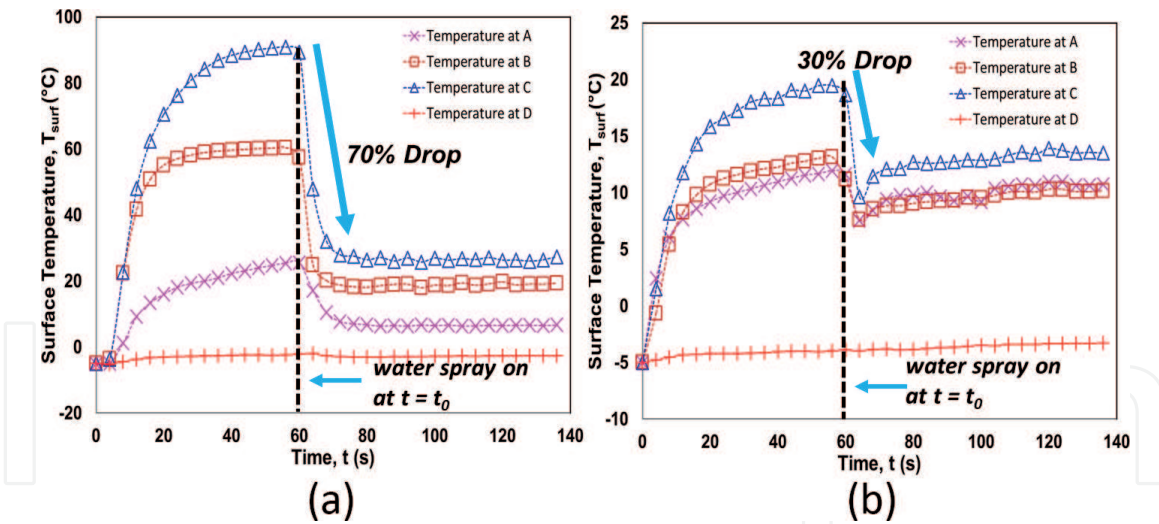


Figure 11. Measured surface temperatures at different chordwise locations on the airfoil surface before and after starting the ice accretion process.

strip-patterned temperature distribution was found over the airfoil surface on electric film heater side at $t = 10$ seconds. Such a strip-like temperature distribution was due to the configuration of the etched foil resistance element encapsulated between the Polyimide films in the electric film heater.

As the time goes by, more and more thermal energy would be generated on both the plasma actuator side and the electric film heater side of the airfoil surface. At about 50 second after turning on the plasma actuator and the electric film heater, a thermal equilibrium state was found to achieve on both sides of the airfoil surface, as indicated by the flattening surface temperature profiles shown in **Figure 11(a)** and **(b)**. It can be seen clearly that, the surface temperatures over the electrical film heater were much higher than those over the DBD plasma actuator as they reached the thermal equilibrium state. The temperatures at the downstream location “C” (*i.e.*, $X/D = 18\%$) were found to be the maximum on both sides with the measured values becoming 20°C and 90°C on the plasma actuator side and the electric film heater side, respectively. As described above, while the thermal energy generated by the electrical film heater is mainly at the heater surface through resistive heating, the primary heating mechanism in DBD plasma actuation is through gas heating and then heating up the dielectric/electrodes surfaces through direct injection, convection and radiation [32]. Therefore, with the same power input, the measured surface temperatures on the electric film heater surface were found to be much higher than those over the DBD plasma actuator. It was also found that, after the thermal equilibrium state was achieved, the temperature was higher at the locations further away from the airfoil leading edge (*i.e.*, $X/C \approx 18\%$) as clearly shown in **Figures 10** and **11**. Existence of such a temperature gradient over the airfoil surface was believed to be caused by the development of the thermal boundary layer over the airfoil surface, *i.e.*, due to the significant convective heat transfer over the airfoil surface with the maximum heat convection locating at the airfoil leading edge and decreasing gradually in the downstream region.

As indicated by the dashed line in **Figure 11**, the water spray system of ISU was switched on at $t = 60$ s to start the ice accretion process, *i.e.*, at 60 seconds after turning on the plasma actuator and the electrical film heater. This time instant was also defined as t_0 , as given in **Figure 10(b)**. It was found that, after the super-cooled water droplets impinged onto the airfoil surface, for the time instance at $t = t_0 + 25$ s, while the surface temperature on the electric film heater was found to decrease significantly, the temperature on the surface of the plasma actuator only dropped

slightly as shown in **Figure 10**. As the time goes on, more and more impinged water would be collected on the airfoil surface. Since the power input to the plasma actuator and the electrical film heater were sufficiently high to prevent ice accretion over the airfoil surfaces (i.e., $P_d = 15.6 \text{ kW/m}^2$), the mass transport and energy transfer on both sides of the airfoil surface were found to reach an equilibrium state, as indicated by the almost unchanged temperature distributions. More quantitatively, after the water droplets impinged on the airfoil surface, while the temperature drop on the airfoil surface protected by the plasma actuator was about 33% (i.e., the temperature dropped from 12.0°C to 8.0°C at the location A and B, and dropped from 18.0°C to 12.0°C at the location C), the corresponding temperature decrease on the airfoil surface protected by the electrical film heater were found to be around 70% (i.e., the temperature decreased from 25.0°C to 6.0°C at the location A, from 60.0°C to 20.0°C at the location B, and from 90.0°C to 25.0°C at the location C). Such significant differences in the surface temperature changes before and after the impingement of the super-cooled water droplets can be explained by the different heating mechanisms discussed in the previous section. For the electrical film heater case, since the thermal energy was mainly generated at the heater surface, and then transferred into the impinged supercooled water droplets, the measured surface temperature, therefore, appeared to drop significantly due to the great temperature differences between the heater surface and the impinged water droplets. However, for the case with the water droplets impinging onto the surface of the DBD plasma actuator, the water droplets had already been effectively warmed up through the forced heat convection as they were flying through the hot air above the plasma actuator. Since the temperatures of the water droplets would be increased substantially before impacting onto the dielectric/electrodes surface, it results in the much smaller surface temperature drops upon the impacting of the water droplets onto the airfoil surface protected by the plasma actuator, as revealed quantitatively in **Figure 11(b)**.

4.4 Further improve the anti-/de-icing performance of the DBD plasma-based approach with a duty-cycle modulation technique

As described above, with the same power input, the DBD plasma-based approach was demonstrated to be more effective in preventing ice accretion over the airfoil surface, in comparison with the conventional electrical heating method. The anti-/de-icing performance of the DBD plasma-based approach can be further improved through optimization of the design paradigms of the plasma actuation in the terms of plasma actuation modes (i.e., AC-DBD vs. ns-DBD plasma actuation) [38], the layout design of the plasma actuator over the airfoil surface [36], the applied voltage and frequency, etc. [51]. As an example of the attempts to optimize the DBD plasma actuation for improved anti-/de-icing performance, a duty-cycled modulation concept was utilized by leveraging the unique feature of fast response time for the DBD plasma actuation (i.e., on the order of $10 \sim 100 \text{ ms}$) in terms of momentum transfer [28] and thermal effects [47] induced by plasma discharges. **Figure 12** shows a schematic of the duty-cycle modulation from a continuous DBD plasma actuation to a duty-cycled DBD plasma actuation. Various frequencies of the duty-cycled DBD plasma actuation were examined to evaluate the effects of the duty cycle frequency on the thermal characteristics of the DBD plasma actuation [39].

Figure 13 shows the comparison of the acquired ice accretion images and the corresponding IR thermal imaging results with the DBD plasma actuators being operated at different duty-cycled frequencies. The experimental study was conducted under the same icing test condition of the test conditions of $U_\infty = 40 \text{ m/s}$, $T_\infty = -5^\circ\text{C}$ and $LWC = 1.0 \text{ g/m}^3$. While the maximum instantaneous power inputs

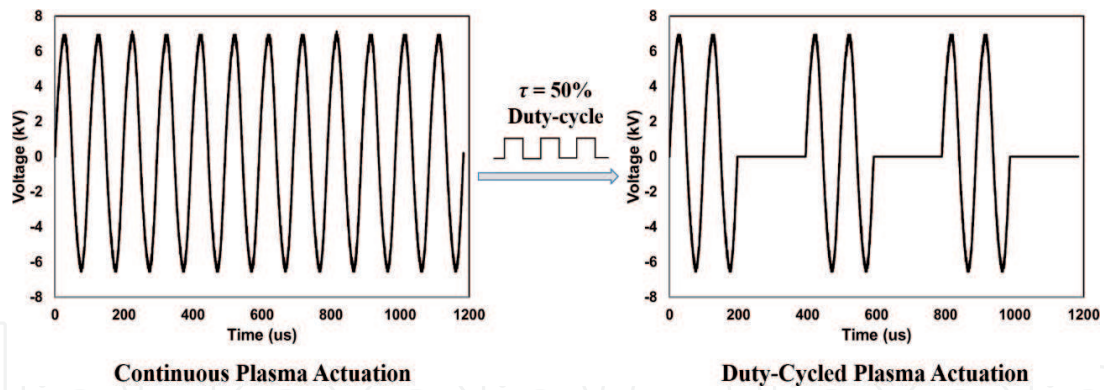


Figure 12. A schematic of the modulation from a continuous plasma actuation to a duty-cycled plasma actuation for improved anti-/de-icing performance.

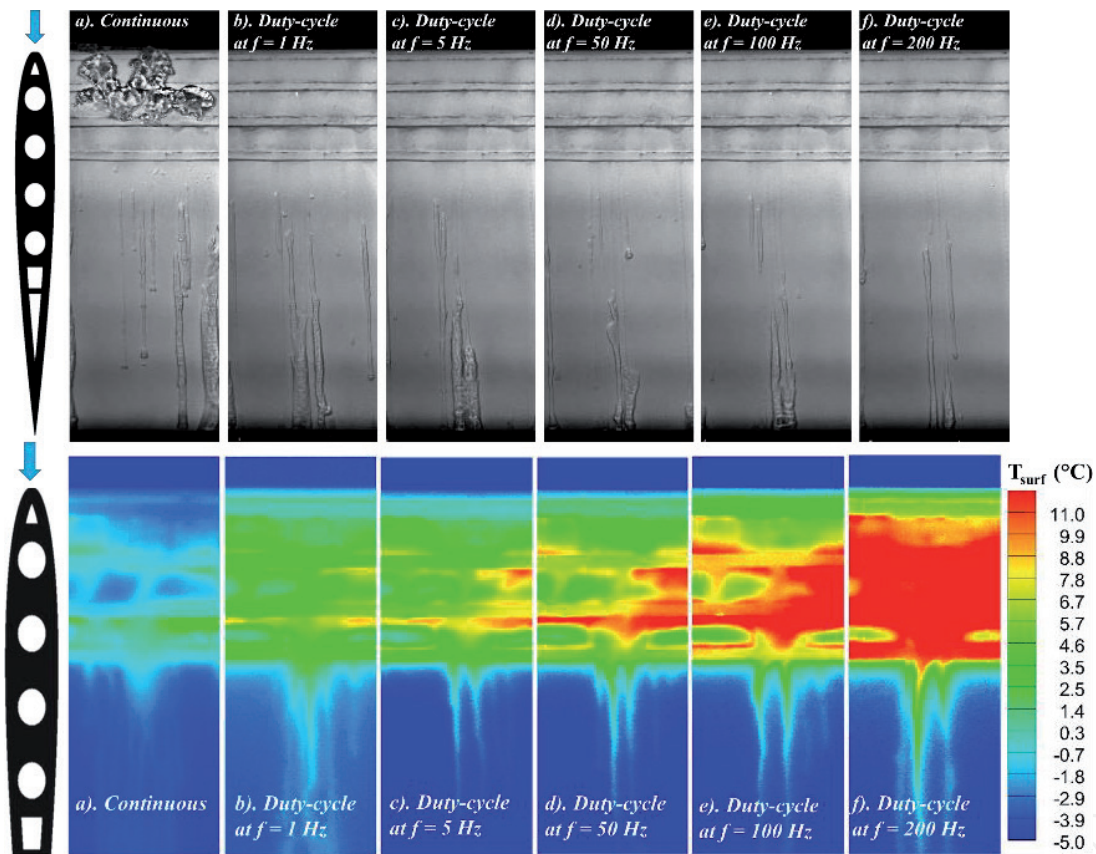


Figure 13. Comparison of duty-cycled DBD plasma actuations modulated with different duty-cycle frequencies.

supplied to the plasma actuator were different for the cases with different duty-cycle modulation frequencies, the total power consumptions over a given period of time were kept at the same level for all the compared cases. It is clearly seen that, the cases with duty-cycled plasma actuations show much better anti-/de-icing performance (i.e., with the plasma region being completely free of ice), in comparison to that of the continuous plasma actuation (i.e., the baseline case shown at the most left side of **Figure 13**). As the duty cycle frequency increases, much less rivulets-shaped ice features were found to form over the airfoil surface. Since the surface temperatures for the cases with the duty cycled DBD plasma actuations are much higher than that of the baseline case with continuous plasma actuation, the increase in the duty cycle frequency was found to further enhance the thermal effects of the DBD plasma actuation, resulting in higher temperatures over the airfoil surface, as revealed quantitatively from the acquired IR thermal imaging results. The

enhanced thermal effects of the duty-cycled DBD plasma actuation at higher duty cycle frequencies was demonstrated to be able to further improve the anti-/de-icing performance of the DBD-plasma-based approach for aircraft icing mitigation.

5. Conclusion

In the present study, we report the research progress made in our efforts to utilize the thermal effects induced by DBD plasma actuation to suppress dynamic ice accretion process over the surface of an airfoil/wing model for aircraft icing mitigation. While the fundamental mechanisms for thermal energy generation in DBD plasma actuation were introduced briefly, the significant differences in the working mechanism of the DBD-plasma-based surface heating approach from those of conventional resistive electric heating methods were highlighted for aircraft anti-/de-icing applications. By leveraging the unique Icing Research Tunnel available at Iowa State University (*i.e.*, ISU-IRT), a comprehensive experimental campaign was conducted to quantify the thermodynamic characteristics of an DBD plasma actuator embedded over the surface of an airfoil model exposed to frozen cold incoming airflow coupled with significant convective heat transfer in the context of aircraft anti-/de-icing. By integrating a DBD plasma actuator and a conventional electrical film heater onto the same airfoil/wing model, an experimental investigation was conducted to provide a side-by-side comparison between the DBD plasma-based approach and conventional resistive electrical heating method in preventing ice formation and accretion over the airfoil surface under a typical aircraft icing condition. While a high-speed camera was used to capture the transient details of the dynamic ice accretion and water transport processes over the airfoil surface, an infrared (IR) thermal imaging system was utilized to map the corresponding temperature over the airfoil surface protected by the DBD plasma actuator and the electrical film heater during the anti-/de-icing operation. Based on the side-by-side comparison of the measurement results (*i.e.*, snapshots of the visualization images and quantitative surface temperature distributions) on the plasma side of the airfoil surface against those of the electric film heater side under the same icing test condition, the effectiveness of using the thermal effects induced by DBD plasma actuation and the conventional electrical heating in preventing ice formation and accretion over the airfoil surface was evaluated and analyzed in details.

It was found that, with the same input power density, the surface temperature on the electric film heater was much higher than that over the surface of the DBD plasma actuator before the water droplets impingement, which was essentially due to the different heating mechanisms of the two methods. For the conventional electrical film heater, the thermal energy was mainly generated at the heater surface. For the case of the DBD plasma actuation, the heating path is through heat transfer from the plasma discharges to the ambient gas at first, and then heating up the surfaces of the dielectric layer and electrodes through direct injection, convection, and radiation. Upon the impingement of the super-cooled water droplets onto the airfoil surface, while the surface temperature over the electrical film heater was found to descend significantly due to the instant heat transfer from the electric film heater surface to the impinged water mass, the decrease in the measured surface temperature over the airfoil surface on the plasma actuator side appeared to be much less since the airborne water droplets were pre-heated greatly as flying through the hot air above the DBD plasma actuator before being in contacting with the heated airfoil surface. As a result, the DBD plasma-based method showed a more promising performance in preventing ice formation and accretion over the airfoil surface, in comparison with that of the conventional electrical heating method.

An explorative study was also conducted to further improve the anti-/de-icing performance of the DBD plasma-based method by adopting a duty-cycle modulation concept. It was found that the implementation of duty-cycled modulation to the DBD plasma actuation can significantly enhance the thermal effects induced by the DBD plasma actuation. It was demonstrated clearly that, under the same icing condition and the same total power input, the duty-cycled plasma actuation has a better anti-/de-icing performance in comparison to the continuous plasma actuation. The findings derived from the present study could be used to explore/optimize design paradigm for the development of novel DBD-plasma-based anti-/de-icing strategies tailored specifically for aircraft icing mitigation.

Acknowledgements

The research work is partially supported by Iowa Energy Center for Wind Turbine Icing Study under the IEC Competitive Grant # 312350 and National Science Foundation (NSF) under award numbers of CBET-1935363 and CBET-1916380.

Author details

Cem Kolbakir^{1,2}, Haiyang Hu¹, Yang Liu^{1,3} and Hui Hu^{1*}


1 Department of Aerospace Engineering, Iowa State University, Ames, IA, USA

2 Department of Aerospace Engineering, Samsun University, Samsun, Turkey

3 Department of Engineering, East Carolina University, Greenville, USA

*Address all correspondence to: huhui@iastate.edu

IntechOpen

© 2021 The Author(s). Licensee IntechOpen. This chapter is distributed under the terms of the Creative Commons Attribution License (<http://creativecommons.org/licenses/by/3.0>), which permits unrestricted use, distribution, and reproduction in any medium, provided the original work is properly cited. 

References

- [1] Korkan, K. D., Dadone, L., and Shaw, R. J. "Helicopter Rotor Performance Degradation in Natural Icing Encounter." *Journal of Aircraft*, Vol. 21, No. 1, 1984, pp. 84-85. <https://doi.org/10.2514/3.48226>.
- [2] Thomas, S. K., Cassoni, R. P., and MacArthur, C. D. "Aircraft Anti-Icing and de-Icing Techniques and Modeling." *Journal of Aircraft*, Vol. 33, No. 5, 1996, pp. 841-854. <https://doi.org/10.2514/3.47027>.
- [3] Cebeci, T., and Kafyeke, F. "AIRCRAFT ICING." *Annual Review of Fluid Mechanics*, Vol. 35, No. 1, 2003, pp. 11-21. <https://doi.org/10.1146/annurev.fluid.35.101101.161217>.
- [4] Bragg, M. B., Broeren, A. P., and Blumenthal, L. A. "Iced-Airfoil Aerodynamics." *Progress in Aerospace Sciences*, Vol. 41, No. 5, 2005, pp. 323-362. <https://doi.org/10.1016/j.paerosci.2005.07.001>.
- [5] Heinrich, A., Ross, R., Zumwalt, G., Provorse, J., and Padmanabhan, V. *Aircraft Icing Handbook. Volume 2*. Gates LwarJet Corp, Wichita, KS, 1991.
- [6] Gray, L. Review of Aircraft Deicing and Anti-Icing Fluid Storm Water Runoff Control Technologies. 2013.
- [7] Kent, R., and Andersen, D. "Canadian Water Quality Guidelines for Glycols—An Ecotoxicological Review of Glycols and Associated Aircraft Anti-Icing and Deicing Fluids." *Environmental Toxicology*, Vol. 14(5), 1999, pp. 481-522.
- [8] Thomas, S. K., Cassoni, R. P., and MacArthur, C. D. "Aircraft Anti-Icing and de-Icing Techniques and Modeling." *Journal of Aircraft*, Vol. 33(5), 2012, pp. 841-854.
- [9] Lin, Y., Chen, H., Wang, G., and Liu, A. "Coatings Recent Progress in Preparation and Anti-Icing Applications of Superhydrophobic Coatings." <https://doi.org/10.3390/coatings8060208>.
- [10] Antonini, C., Innocenti, M., Horn, T., Marengo, M., and Amirfazli, A. "Understanding the Effect of Superhydrophobic Coatings on Energy Reduction in Anti-Icing Systems." *Cold Regions Science and Technology*, Vol. 67, Nos. 1-2, 2011, pp. 58-67. <https://doi.org/10.1016/j.coldregions.2011.02.006>.
- [11] Zhang, Z., Ma, L., Liu, Y., and Hu, H. "An Experimental Study on the Durability of a Hydro-/Ice-Phobic Surface Coating for Aircraft Icing Mitigation." *2018 Atmospheric and Space Environments Conference*, 2018, pp. 1-15. <https://doi.org/10.2514/6.2018-3655>.
- [12] Antonini, C., Innocenti, M., Horn, T., Marengo, M., and Amirfazli, a. "Understanding the Effect of Superhydrophobic Coatings on Energy Reduction in Anti-Icing Systems." *Cold Regions Science and Technology*, Vol. 67, Nos. 1-2, 2011, pp. 58-67. <https://doi.org/10.1016/j.coldregions.2011.02.006>.
- [13] Gao, L., Liu, Y., Ma, L., and Hu, H. "A Hybrid Strategy Combining Minimized Leading-Edge Electric-Heating and Superhydro-/Ice-Phobic Surface Coating for Wind Turbine Icing Mitigation." *Renewable Energy*, Vol. 140, 2019, pp. 943-956. <https://doi.org/10.1016/J.RENENE.2019.03.112>.
- [14] Wang, J.-J., Choi, K.-S., Feng, L.-H., Jukes, T. N., and Whalley, R. D. "Recent Developments in DBD Plasma Flow Control." *Progress in Aerospace Sciences*, Vol. 62, 2013, pp. 52-78. <https://doi.org/10.1016/j.paerosci.2013.05.003>.
- [15] Ebrahimi, A., and Movahhedi, M. "Power Improvement of NREL 5-MW Wind Turbine Using Multi-DBD Plasma Actuators." *Energy Conversion and Management*, Vol. 146, 2017, pp. 96-106. <https://doi.org/10.1016/j.enconman.2017.05.019>.

- [16] Meng, X., Hu, H., Yan, X., Liu, F., and Luo, S. "Lift Improvements Using Duty-Cycled Plasma Actuation at Low Reynolds Numbers." *Aerospace Science and Technology*, Vol. 72, 2018. <https://doi.org/10.1016/j.ast.2017.10.038>.
- [17] Roupasov, D. V., Nikipelov, A. A., Nudnova, M. M., and Starikovskii, A. Y. "Flow Separation Control by Plasma Actuator with Nanosecond Pulsed-Periodic Discharge." *AIAA Journal*, Vol. 47, No. 1, 2009, pp. 168-185. <https://doi.org/10.2514/1.38113>.
- [18] Correale, G., Michelis, T., Ragni, D., Kotsonis, M., and Scarano, F. "Nanosecond-Pulsed Plasma Actuation in Quiescent Air and Laminar Boundary Layer." *Journal of Physics D: Applied Physics*, Vol. 47, No. 10, 2014, p. 105201. <https://doi.org/10.1088/0022-3727/47/10/105201>.
- [19] SAMIMY, M., KIM, J.-H., KASTNER, J., ADAMOVICH, I., and UTKIN, Y. "Active Control of High-Speed and High-Reynolds-Number Jets Using Plasma Actuators." *Journal of Fluid Mechanics*, Vol. 578, 2007, p. 305. <https://doi.org/10.1017/S0022112007004867>.
- [20] Aleksandrov, N. L., Kindysheva, S. V., Nudnova, M. M., and Starikovskiy, A. Y. "Mechanism of Ultra-Fast Heating in a Non-Equilibrium Weakly Ionized Air Discharge Plasma in High Electric Fields." *Journal of Physics D: Applied Physics*, Vol. 43, No. 25, 2010, p. 255201. <https://doi.org/10.1088/0022-3727/43/25/255201>.
- [21] Little, J., Takashima, K., Nishihara, M., Adamovich, I., and Samimy, M. "Separation Control with Nanosecond-Pulse-Driven Dielectric Barrier Discharge Plasma Actuators." *AIAA Journal*, Vol. 50, No. 2, 2012, pp. 350-365. <https://doi.org/10.2514/1.J051114>.
- [22] Benard, N., and Moreau, E. "On the Vortex Dynamic of Airflow Reattachment Forced by a Single Non-Thermal Plasma Discharge Actuator." *Flow, Turbulence and Combustion*, Vol. 87, No. 1, 2011, pp. 1-31. <https://doi.org/10.1007/s10494-011-9325-4>.
- [23] Little, J., Nishihara, M., Adamovich, I., and Samimy, M. "High-Lift Airfoil Trailing Edge Separation Control Using a Single Dielectric Barrier Discharge Plasma Actuator." *Experiments in Fluids*, Vol. 48, No. 3, 2010, pp. 521-537. <https://doi.org/10.1007/s00348-009-0755-x>.
- [24] Jousot, R., Hong, D., Weber-Rozenbaum, R., and Leroy-Chesneau, A. Modification of the Laminar-to-Turbulent Transition on a Flat Plate Using DBD Plasma Actuator. In *5th Flow Control Conference*, American Institute of Aeronautics and Astronautics, 2010.
- [25] Duchmann, A., Grundmann, S., and Tropea, C. "Delay of Natural Transition with Dielectric Barrier Discharges." *Experiments in Fluids*, Vol. 54, No. 3, 2013, p. 1461. <https://doi.org/10.1007/s00348-013-1461-2>.
- [26] Corke, T. C., Enloe, C. L., and Wilkinson, S. P. "Dielectric Barrier Discharge Plasma Actuators for Flow Control." *Annual Review of Fluid Mechanics*, Vol. 42, No. 1, 2010, pp. 505-529. <https://doi.org/10.1146/annurev-fluid-121108-145550>.
- [27] Thomas, F. O., Corke, T. C., Iqbal, M., Kozlov, A., and Schatzman, D. "Optimization of Dielectric Barrier Discharge Plasma Actuators for Active Aerodynamic Flow Control." *AIAA Journal*, Vol. 47, No. 9, 2009, pp. 2169-2178. <https://doi.org/10.2514/1.41588>.
- [28] Benard, N., and Moreau, E. "Electrical and Mechanical Characteristics of Surface AC Dielectric Barrier Discharge Plasma Actuators Applied to Airflow Control." *Experiments in Fluids*, Vol. 55, No. 11, 2014, p. 1846. <https://doi.org/10.1007/s00348-014-1846-x>.
- [29] Liu, Y., Kolbakir, C., Starikovskiy, A. Y., Miles, R., and Hu, H. "An

Experimental Study on the Thermal Characteristics of NS-DBD Plasma Actuation and Application for Aircraft Icing Mitigation.” *Plasma Sources Science and Technology*, Vol. 28, No. 1, 2019, p. 014001. <https://doi.org/10.1088/1361-6595/aaedf8>.

[30] Stanfield, S. A., Menart, J., DeJoseph, C., Kimmel, R. L., and Hayes, J. R. “Rotational and Vibrational Temperature Distributions for a Dielectric Barrier Discharge in Air.” *AIAA Journal*, Vol. 47, No. 5, 2009, pp. 1107-1115. <https://doi.org/10.2514/1.37648>.

[31] Dong, B., Bauchire, J. M., Pouvesle, J. M., Magnier, P., and Hong, D. “Experimental Study of a DBD Surface Discharge for the Active Control of Subsonic Airflow.” *Journal of Physics D: Applied Physics*, Vol. 41, No. 15, 2008, p. 155201. <https://doi.org/10.1088/0022-3727/41/15/155201>.

[32] Tirumala, R., Benard, N., Moreau, E., Fenot, M., Lalizel, G., and Dorignac, E. “Temperature Characterization of Dielectric Barrier Discharge Actuators: Influence of Electrical and Geometric Parameters.” *Journal of Physics D: Applied Physics*, Vol. 47, No. 25, 2014, p. 255203. <https://doi.org/10.1088/0022-3727/47/25/255203>.

[33] Cai, J., Tian, Y., Meng, X., Han, X., Zhang, D., and Hu, H. “An Experimental Study of Icing Control Using DBD Plasma Actuator.” *Experiments in Fluids*, Vol. 58, No. 8, 2017, p. 102. <https://doi.org/10.1007/s00348-017-2378-y>.

[34] Corke, T. C., Enloe, C. L., and Wilkinson, S. P. “Dielectric Barrier Discharge Plasma Actuators for Flow Control.” *Annual Review of Fluid Mechanics*, Vol. 42, No. 1, 2010, pp. 505-529. <https://doi.org/10.1146/annurev-fluid-121108-145550>.

[35] Zhou, W., Liu, Y., Hu, H., Hu, H., and Meng, X. “Utilization of Thermal

Effect Induced by Plasma Generation for Aircraft Icing Mitigation.” *AIAA Journal*, Vol. 56, No. 3, 2018, pp. 1097-1104. <https://doi.org/10.2514/1.J056358>.

[36] Kolbakir, C., Hu, H., Liu, Y., and Hu, H. “An Experimental Study on Different Plasma Actuator Layouts for Aircraft Icing Mitigation.” *Aerospace Science and Technology*, Vol. 107, 2020, p. 106325. <https://doi.org/10.1016/j.ast.2020.106325>.

[37] Meng, X., Hu, H., Li, C., Abbasi, A. A., Cai, J., and Hu, H. “Mechanism Study of Coupled Aerodynamic and Thermal Effects Using Plasma Actuation for Anti-Icing.” *Physics of Fluids*, Vol. 31, No. 3, 2019. <https://doi.org/10.1063/1.5086884>.

[38] Liu, Y., Kolbakir, C., Hu, H., Starikovskiy, A., and Miles, R. B. “An Experimental Study on the Thermal Characteristics of NS-DBD Plasma Actuation and Application for Aircraft Icing Mitigation.” *Plasma Sources Science and Technology*, 2018. <https://doi.org/10.1088/1361-6595/aaedf8>.

[39] Liu, Y., Kolbakir, C., Hu, H., Meng, X., and Hu, H. “An Experimental Study on the Thermal Effects of Duty-Cycled Plasma Actuation Pertinent to Aircraft Icing Mitigation.” *International Journal of Heat and Mass Transfer*, Vol. 136, 2019. <https://doi.org/10.1016/j.ijheatmasstransfer.2019.03.068>.

[40] Jousset, R., Boucinha, V., Weber-Rozenbaum, R., Rabat, H., Leroy-Chesneau, A., and Hong, D. Thermal Characterization of a DBD Plasma Actuator: Dielectric Temperature Measurements Using Infrared Thermography. 2010.

[41] Starikovskii, A. Y., Nikipelov, A. A., Nudnova, M. M., and Roupasov, D. V. “SDBD Plasma Actuator with Nanosecond Pulse-Periodic Discharge.” *Plasma Sources Science and Technology*, Vol. 18, No. 3, 2009, p. 034015. <https://doi.org/10.1088/0963-0252/18/3/034015>.

- [42] Zhu, Y., Wu, Y., Cui, W., Li, Y., and Jia, M. "Numerical Investigation of Energy Transfer for Fast Gas Heating in an Atmospheric Nanosecond-Pulsed DBD under Different Negative Slopes." *Journal of Physics D: Applied Physics*, Vol. 46, No. 49, 2013, p. 495205. <https://doi.org/10.1088/0022-3727/46/49/495205>.
- [43] Leonov, S. B., Petrishchev, V., and Adamovich, I. V. "Dynamics of Energy Coupling and Thermalization in Barrier Discharges over Dielectric and Weakly Conducting Surfaces on μ s to Ms Time Scales." *Journal of Physics D: Applied Physics*, Vol. 47, No. 46, 2014, p. 465201. <https://doi.org/10.1088/0022-3727/47/46/465201>.
- [44] Popov, N. A. "Investigation of the Mechanism for Rapid Heating of Nitrogen and Air in Gas Discharges." *Plasma Physics Reports*, Vol. 27, No. 10, 2001, pp. 886-896. <https://doi.org/10.1134/1.1409722>.
- [45] Conrads, H., and Schmidt, M. "Plasma Generation and Plasma Sources." *Plasma Sources Science and Technology*, Vol. 9, No. 4, 2000, pp. 441-454. <https://doi.org/10.1088/0963-0252/9/4/301>.
- [46] Li, H., Chen, F., and Hu, H. "Simultaneous Measurements of Droplet Size, Flying Velocity and Transient Temperature of in-Flight Droplets by Using a Molecular Tagging Technique." *Experiments in Fluids*, Vol. 56, No. 10, 2015, p. 194. <https://doi.org/10.1007/s00348-015-2063-y>.
- [47] Rodrigues, F., Pascoa, J., and Trancossi, M. "Heat Generation Mechanisms of DBD Plasma Actuators." *Experimental Thermal and Fluid Science*, Vol. 90, 2018, pp. 55-65. <https://doi.org/10.1016/J.EXPTHERMFLUSCI.2017.09.005>.
- [48] Waldman, R. M., and Hu, H. "High-Speed Imaging to Quantify Transient Ice Accretion Process over an Airfoil." *Journal of Aircraft*, Vol. 53, No. 2, 2015, pp. 369-377. <https://doi.org/10.2514/1.C033367>.
- [49] Incropera, F. P. *Fundamentals of Heat and Mass Transfer*. BOOK. John Wiley & Sons, 2011.
- [50] Liu, Y., Kolbakir, C., Hu, H., and Hu, H. "A Comparison Study on the Thermal Effects in DBD Plasma Actuation and Electrical Heating for Aircraft Icing Mitigation." *International Journal of Heat and Mass Transfer*, Vol. 124, 2018, pp. 319-330. <https://doi.org/10.1016/J.IJHEATMASSTRANSFER.2018.03.076>.
- [51] Liu, Y., Kolbakir, C., Hu, H., Starikovskiy, A. Y., and Miles, R. "A Parametric Study to Explore Ns-DBD Plasma Actuation for Aircraft Icing Mitigation." 2018. <https://doi.org/10.2514/6.2018-3756>.